Scripta Materialia 264 (2025) 116721

Contents lists available at ScienceDirect

Scripta Materialia

journal homepage: www.journals.elsevier.com/scripta-materialia

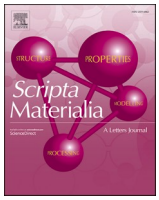

Joule heating enables ultra-fast SiC ceramics joining in seconds

Jie Xu [a,b], Xiaobing Zhou [a,b,*], Qing Huang [a,b,*]

[a] Zhejiang Key Laboratory of Data-Driven High-Safety Energy Materials and Applications, Ningbo Key Laboratory of Special Energy Materials and Chemistry, Ningbo Institute of Materials Technology and Engineering, Chinese Academy of Sciences, Ningbo 315201, China
[b] University of Chinese Academy of Sciences, Beijing 100049, China

ARTICLE INFO

Keywords:
SiC ceramics
Joining
Joule heating
Interface reaction
Aluminum

ABSTRACT

Reliable ultra-fast pressure-less joining of Silicon Carbide (SiC) ceramic is a critical challenge for extreme environment applications. This study presents a novel approach for ultra-fast, pressure-less joining of SiC ceramics. Utilizing the resistance increase owing to the interface reaction at the interlayer, an ultra-fast Joule heating technique enabled robust SiC joints in just 23 s without external preheating. A 5-micron-thick aluminum foil was used as the initial joining layer, undergoing a rapid interface reaction to generate high-resistance compounds, such as Al_4C_3, Al_4SiC_4, and Al_2OC during the flash heating process. This localized heating, which inhibited the energy dissipation in heating the entire joint assembly, facilitated the creation of strong SiC joints within seconds without pre-heating, achieving a shear strength up to 76 ± 12 MPa. The proposed joining method, utilizing the inherent resistance changes within the interlayer, demonstrates significant potential for joining other non-conductive ceramics effectively.

Silicon carbide (SiC) exhibits a relatively low density, excellent high-temperature mechanical properties, as well as outstanding oxidation, corrosion and irradiation damage resistance [1–3]. Therefore, it is considered a promising candidate for applications in aviation and aerospace industries, or advanced nuclear reactors [4–8]. However, the wider application of SiC-based components depends on the ability to join them, since the fabrication of large-size SiC components with complex shapes still constitutes a significant technological challenge [9–11]. A primary example is the joining of SiC cladding tube and the end cap in advanced nuclear reactors [12–13].

Therefore, a number of SiC joining techniques have been developed, including brazing [14–16], solid state diffusion joining [17], nano-infiltration and transient eutectic (NITE) liquid phase joining [18], glass and glass-ceramic joining [19], pre-ceramic polymer routes [20], MAX phase joining [21–24]. and $RE_3Si_2C_2$ near seamless joining [25–29]. In addition, an electric current assisted joining technique was used to join SiC and/or C_f/SiC composites, as the applied electric current facilitates the atomic diffusion and interface reaction [16,30]. It was reported that the electric current assisted technique was successfully used to form seamless SiC joints using Yb_3SiC_2 joining layer at a temperature of 1500 °C for 10 min[25]. It should be pointed out that a significant portion of the energy was dissipated in heating the entire joint assembly. Consequently, achieving sound joints typically required high temperatures, extended holding times, and substantial uniaxial pressure (50 MPa) [25–26,28].

Recently, inspired by flash sintering technology [31–36], a novel flash joining technique was used to join SiC in 100 s in air when Ag-Cu-Ti alloy was used as the joining layer, or 30 min when the joining was performed without any joining layer [16,37]. The assisted environment temperature (around 400 °C), along with the inspired electric field, were needed to stimulate the flash joining [16,37–38]. Yoshitake et al. [39]. employed flash-bonding to join SiC, utilizing a tungsten mesh for heating and the borosilicate glass as a brazing material. Their study focused on the interfacial reactions and wetting behavior between the borosilicate glass and SiC matrix (both as-is and surface-oxidized), but the mechanical properties of the joints were not reported. To the best knowledge of the authors, very few studies have demonstrated ultra-fast SiC joining achieved solely through direct local Joule heating of the joining layer, eliminating the need for an assisted environment temperature and external pressure.

According to the Joule's law, the generated heat is directly proportional to the electrical resistance. Based on this principle, a novel strategy for ultra-fast, localized Joule heating of the joining layer was

* Corresponding authors.
E-mail addresses: zhouxb@nimte.ac.cn (X. Zhou), huangqing@nimte.ac.cn (Q. Huang).

https://doi.org/10.1016/j.scriptamat.2025.116721
Received 6 February 2025; Received in revised form 17 April 2025; Accepted 17 April 2025
Available online 24 April 2025

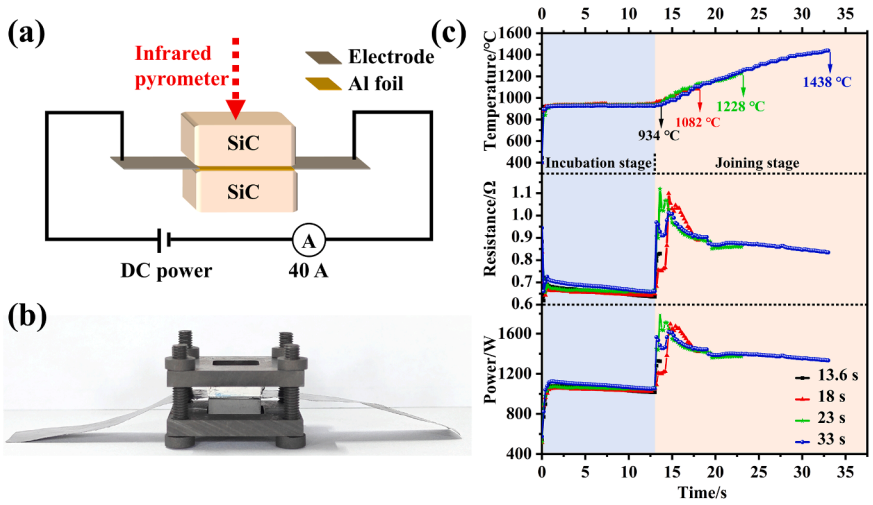

Fig. 1. (a) schematic illustration of the joining set-up; (b) photograph of the joining set-up; (c) variation in resistance, power and temperature as a function of joining time.

proposed in the present work to join SiC. This approach utilizes the significant resistance increase associated with phase transformations generated via interface reactions within the joining layer to effectively join SiC with a minimum external pressure. Due to its low electrical resistance, aluminum can react with SiC to form high electrical resistance phases, such as Al_4C_3 and Al-Si-C. This rapid generation of localized Joule heat facilitates the formation of a strong SiC joint within seconds. Therefore, a 5 μm thick Al foil was designed as an initial joining layer. A constant current of 40 A was applied to heat the Al foil to join SiC ceramics within 13.6–33 s. The influence of joining time on the interfacial reactions and phase evolution of the joining layer was investigated.

Commercial pressure-less sintered 6H-SiC ceramics (98.5 wt. % purity, with C as the main impurity) with dimensions of 10 × 10 × 4 mm^3 and 10 × 7 × 4 mm^3 was purchased from Ningbo Jutuo Seal Materials Co., Ltd., China as the matrix material. High-purity aluminum foil (99.99 wt. % purity,) with a thickness of 5 μm was obtained from the Institute of High Purity Metallic Materials Co., Ltd., China.

All joining experiments were conducted in a glove box in an Ar atmosphere. The schematic illustration of the joining set-up is shown in Fig. 1a. A SiC/Al/SiC sandwich joint was fixed in a customized graphite mold (Fig. 1b). A constant electric current of 40 A, provided by an A-BF-SS-606P power supply, was directly applied to heat the initial Al foil. The change in the resistance of the joints was calculated based on the

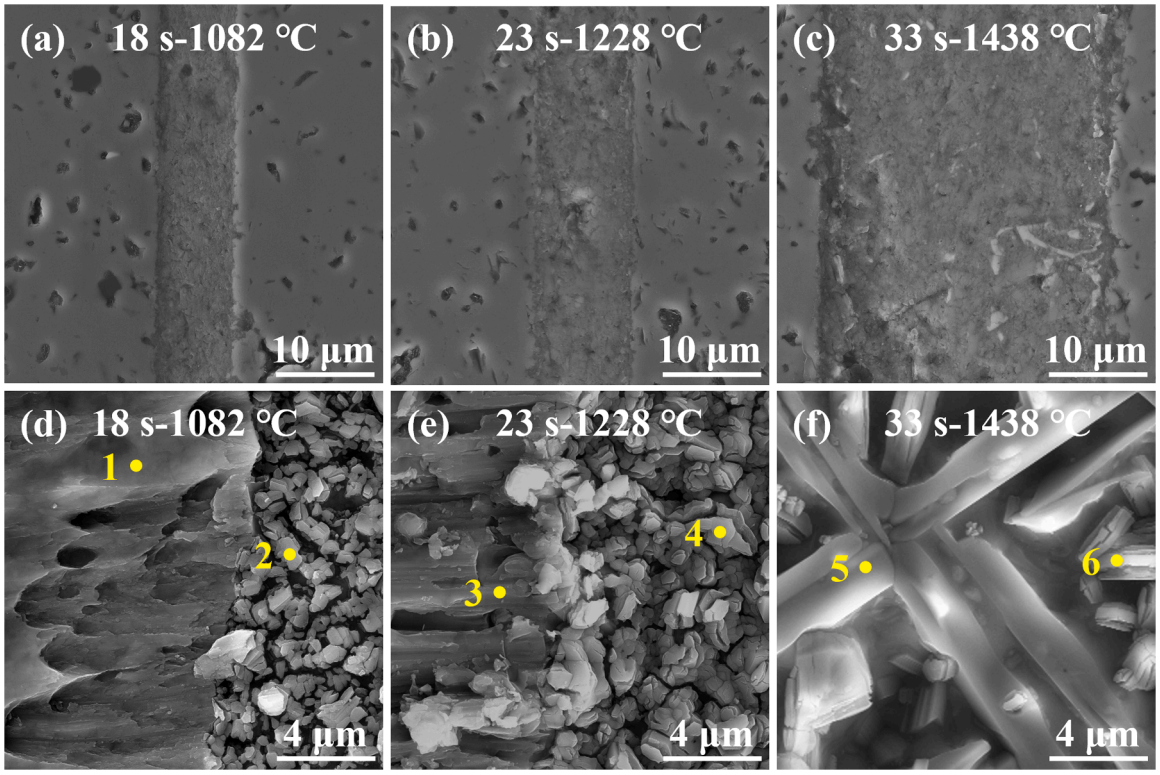

Fig. 2. SEM images of the polished SiC/Al/SiC specimens joined within different times: (a) 18 s, (b) 23 s, (c) 33 s; SEM images of the fracture surfaces of the specimens joined within different times (d) 18 s, (e) 23 s, (f) 33 s.

Table 1
EDS results of the spots 1–6 in Fig. 2.

NO.	Composition in atomic %				Probable phase
	C	Si	Al	O	
1	13	11	74	2	Al
2	23	15	18	44	Al-C/Al-O-C
3	17	21	58	5	Al
4	21	12	21	45	Al-C/Al-O-C
5	41	10	45	4	Al-Si-C
6	24	3	36	37	Al-C/Al-O-C

recorded current-voltage data. The apparent joining temperature was measured on the top SiC surface using an infrared pyrometer. Four different joining times (13.6 s, 18 s, 23 s, and 33 s) corresponding to the measured SiC surface temperatures of 934 °C, 1082 °C, 1228 °C, and 1438 °C, respectively, were investigated to understand the joining mechanism. It is important to note that the actual temperature within the joining layer likely exceeded the measured surface temperature of SiC substrate (potentially surpassing 1715 °C). This is supported by the detection of the Al_2OC phase, which typically forms at temperatures above 1715 °C [40]. Due to the limitations in our current experimental setup, direct in-situ measurement of the interface temperature was not feasible. Future research will focus on refining the temperature measurement methodology to enable more accurate characterization of the thermal conditions at the interface. The variation in resistance, temperature and input power as a function of joining time is shown in Fig. 1c. Based on the depicted curves, the overall joining process can be divided into two distinct stages. Stage I corresponds to the incubation period, when the resistance and temperature remained essentially constant. Stage II is characterized by a sudden increase in joining temperature, attributed to rapid rise in the resistance of the joining layer, possibly arising from a phase transformation generated by the interfacial reactions within the joining layer. After the joining, the power was switched off and the samples were cooled down to room temperature naturally.

The phase composition and the microstructures of the joining layer were investigated using an X-ray diffraction (XRD, D8 Advance, Bruker AXS, Germany), a scanning electron microscope (SEM, Quanta 250 FEG, FEI, USA), and a transmission electron microscope (TEM, Talos™ F200x, Thermo Fisher Scientific, USA) equipped with an energy-dispersive X-ray spectrometry (EDS) detector. The specimens for the TEM observations were machined using a focused ion beam technique (FIB, Auriga, Carl Zeiss). The shear strength at room temperature was measured using a universal electro-mechanical testing system (Zwick Roell, Z250AF, Germany) with a cross-head speed of 0.5 mm/min. At least five samples were measured per each joining parameter and the average value was calculated.

Fig. 2 shows the microstructure of the samples joined within different joining times: 18 s, 23 s and 33 s. Since the sample joined within 13.6 s fell apart during polishing, it was not characterized. Almost no obvious cracks and pores were observed in the joining layer, when the joining time was 18 s and 23 s (Fig. 2a and 2b respectively). On the other hand, some small pores and microcracks propagating perpendicularly to the interface were observed in the sample joined within 33 s (Fig. 2c). The thickness of the interlayer was 7.5 ± 0.2 μm, 8.6 ± 0.2 μm and 29.4 ± 0.3 μm, when the joining time was 18 s, 23 s and 33 s, respectively. The increase in the thickness of the interlayer was primarily attributed to the interface reaction between Al and SiC, which was likely promoted by the increase in temperature as the joining time increased. According to the SEM analysis of the fracture surfaces combined with the EDS analysis, typical layered structures of Al-C and/or Al-O-C phases were detected in the samples joined within 18 s and 23 s (Table 1, point 2 and 4 in Fig. 2d and 2e). On the contrary, the Al-Si-C phase was also observed in the sample joined for 33 s (Table 1, point 5 in Fig. 2f) along with the Al-C and/or Al-O-C phases (Table 1, point 6 in Fig. 2f).

The phase compositions of the joining layer after the joining within different times (temperatures), were further analyzed using XRD and high-resolution transmission electron microscope (HR-TEM) along with semi-quantitative EDS as well as selected area electron diffraction (SAED) analysis. Fig. 3 shows the XRD patterns recorded on the fracture surfaces of the samples joined within various joining times. In the samples joined within 18 s and 23 s, the main generated phases were identified as Si (JCPDS card No 27–1402), Al-O-C (JCPDS card No 36–0148), and $Al_4Si_4C_7$ (JCPDS card No 42–1171), while the matrix of SiC (JCPDS card No 73–1663) and initial Al (JCPDS card No 04–0787) foil were also detected. On the other hand, Al_4C_3 (JCPDS card No 35–0799), Al-O-C and Al_4SiC_4 (JCPDS card No 35–1072) were observed as the main generated phases in the sample joined within 33 s. As the joining time (temperature) increased from 18 s (1082 °C) to 33 s (1438 °C), the relative intensity of the Si diffraction peaks increased, while the intensity of Al peaks decreased. It is likely that Si and Al_4C_3 were formed by the reaction between SiC and Al (reaction 1) [41]. As the joining temperature increased, the content of both Si and Al_4C_3 increased, while the amount of the residual Al decreased. It should be noted that no Al_4C_3 phase was detected in the samples joined within 18 s and 23 s, which might be due to the relatively small amount of Al_4C_3 (lower than the detection limit of XRD). However, the presence of Al_4C_3 in the sample

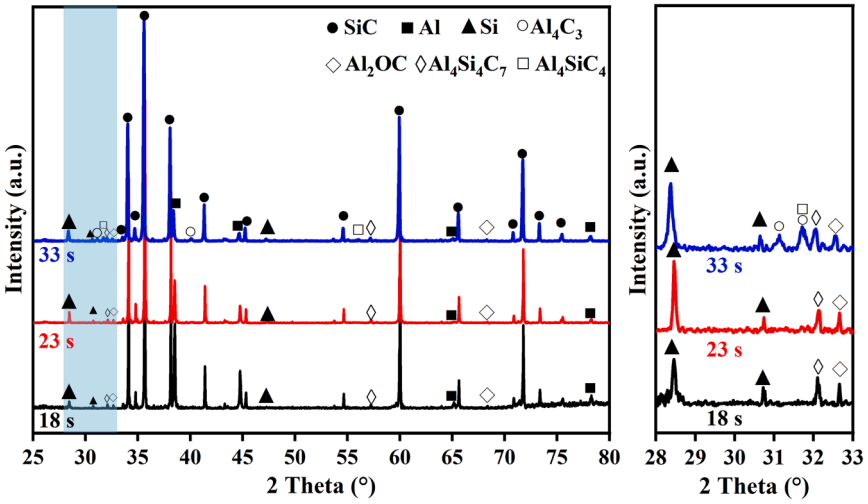

Fig. 3. XRD patterns of the joining layers recorded on the fracture surfaces of SiC/Al/SiC samples joined within different joining times.

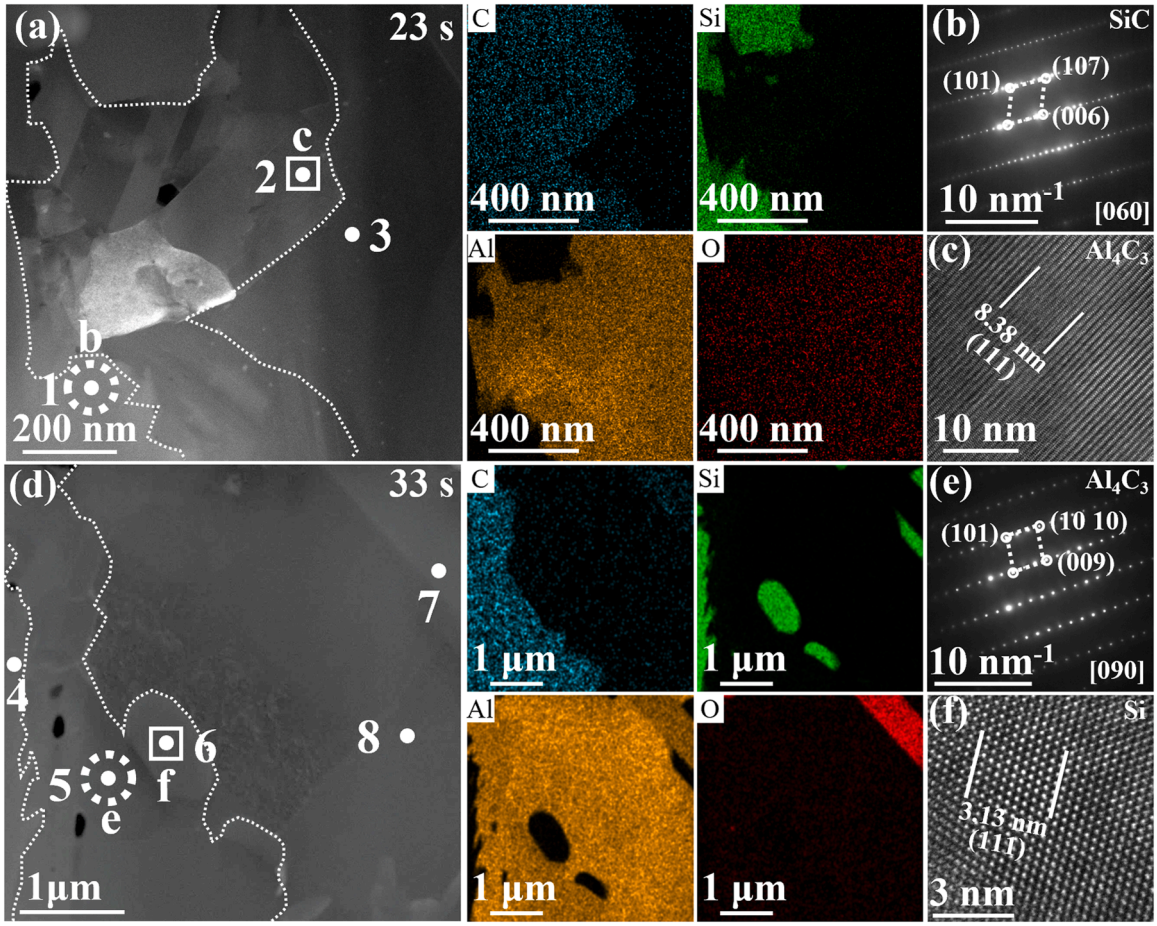

Fig. 4. HAADF images and corresponding elemental distributions of C, Si, Al, and O for the samples joined within 23 s (a) and 33 s (d). SAED patterns of SiC (b) and Al_4C_3 (e), which were taken from the regions highlighted by the dashed white circle in (a) and (d), respectively. The HR-TEM images of the generated Al_4C_3 and Si are shown in (c) and (f), respectively. The white dashed lines in (a) and (d) marked the thickness of Al_4C_3 interface reaction layer.

Table 2
EDS results of points 1–8 in Fig. 4.

NO.	Position	Composition in atomic %				Probable phase
		C	O	Al	Si	
1	matrix	14.71	1.16	1.01	83.12	Si-C
2	Reaction layer	13.31	6.69	77.80	2.20	Al-C
3	Joining layer	0.06	5.99	93.10	0.85	Al
4	matrix	14.86	1.07	1.46	82.61	Si-C
5	Reaction layer	16.45	4.03	77.41	2.12	Al-C
6		0.18	2.55	2.25	95.02	Si
7		12.16	41.02	46.61	0.21	Al-O-C
8	Joining layer	0.35	3.02	96.31	0.31	Al

joined within 23 s was confirmed by the TEM analysis, as shown in Fig. 4a and 4c and Table 2 (point 2). The thickness of the in-situ formed Al_4C_3 reaction layer increased from ~352 nm to ~1870 nm as the joining time (temperature) increased from 23 s (1228 °C) to 33 s (1438 °C). According to the Al-Si-C ternary phase diagram [41–42], it is believed that Al_4SiC_4 was formed by the reaction 2 at the temperature higher than 1450 °C. As shown in Fig. 2f, the typical plate-like morphology of Al_4SiC_4 grains (Table 1, point 5) was observed [43,44]. On the other hand, since the content of the in-situ formed Al_4C_3 in the sample joined within 18 s and 23 s was lower than that of the sample joined in 33 s, only $Al_4Si_4C_7$ was observed, which was formed according to the reaction 3. In addition, the formation of Al_2OC phase could mainly be attributed to the oxidation of Al_4C_3 by the reaction with Al_2O_3, which was likely present on the surface of Al foil (reaction 4) [45]. Lihrmann et al. [40,45] demonstrated that Al_2OC decomposes to Al_4O_4C and Al_4C_3 at 1715 °C, but it can form a metastable Al_2OC phase under rapid cooling conditions. In the present study, the formation of high-resistivity phases at the interface, including Al-C, Al-O-C, and Al-Si-C, increased contact resistance between the Al joining layer and the SiC matrix, leading to the generation of flash Joule heating. Consequently, the actual interface temperature was likely significantly higher than the measured maximum surface temperature of the SiC substrate, potentially exceeding 1715 °C. The following rapid cooling likely facilitated the formation of metastable Al_2OC, which is consistent with the previous works [40,45].

$$4Al + 3SiC \rightarrow Al_4C_3 + 3Si \quad (1)$$

$$Al_4C_3 + SiC \rightarrow Al_4SiC_4 \quad (2)$$

$$Al_4C_3 + 3SiC \rightarrow Al_4Si_4C_7 \quad (3)$$

$$Al_4C_3 + Al_2O_3 \rightarrow 3Al_2OC \quad (4)$$

The joining mechanism could be summarized based on the microstructure and phase evolution of the joining layer. At the beginning stage, the electric current flew directly through the conductive Al foil, which rapidly heated the Al foil to the temperature around 930 °C (Fig. 1b), resulting in the melting of Al foil. Due to the relatively low reaction temperature and the short joining time (13.6 s), an insufficient interfacial reaction occurred, resulting in a weak joint with a shear strength of just 2.5 MPa. As the joining time increased to 18 s and 23 s, the molten Al rapidly reacted with the SiC matrix, resulting in the formation of high-resistance phases, such as Al_4C_3, Al-Si-C, and Al-O-C [46,

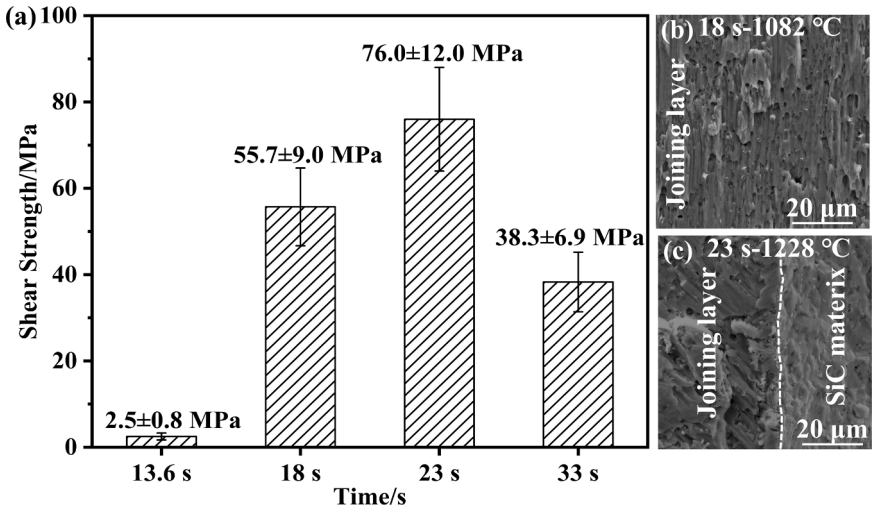

Fig. 5. (a) Shear strength of the SiC/Al/SiC samples joined within different times; SEM images of the fracture surfaces at typical failure position for the samples joined within different joining times: (b) joining layer, 18 s; (c) joining layer and matrix, 23 s.

47]. This reaction caused a significant increase in system resistance, from ~0.63 Ω to ~1.12 Ω (Fig. 1b), leading to the localized Joule heating that greatly facilitated the joining process. It should be mentioned that, at measured SiC surface temperature around 1000 °C, a part of electric current likely flowed through the SiC matrix. This is because the formation of high-resistivity phases (such as Al_4C_3, Al-Si-C, and Al-O-C) at the interface improved the contact resistance between the Al joining layer and SiC matrix, resulting in flash Joule heating. The actual interface temperature was therefore significantly higher than the measured surface temperature. Furthermore, SiC becomes conductive at temperatures above 1000 °C [48], meaning that some electric current likely flowed through the SiC matrix, which promoted chemical bonding. Additionally, the thermal expansion coefficients of Al_4C_3 (5.0×10^{-6} K^{-1}) and Al_4SiC_4 (6.2×10^{-6} K^{-1}) are intermediate between Al (25.9×10^{-6} K^{-1}) and SiC (4.7×10^{-6} K^{-1}), which helps to mitigate thermal residual stresses caused by the thermal mismatch [49–51]. In addition, the in-situ formed nano-sized Al_4C_3, Al-Si-C and Al-O-C ceramic particles (Fig. 2d, 2e and Fig. 4a) could reinforce the residual Al joining layer. Therefore, the shear strength of the joints increased from 55.7 ± 9 MPa to 76 ± 12 MPa as the joining time (temperature) increased from 18 s (1082 °C) to 23 s (1228 °C) (Fig. 5a). Failure mainly occurred in the joining layer for the sample joined at 18 s, while for the sample joined at 23 s the combined failure in the joining layer and SiC matrix was observed (Fig. 5b and Fig. 5c). On the other hand, as the joining time (temperature) further increased to 33 s (1438 °C), the ~1870 nm thick Al_4C_3 layer with a relatively large plate-like Al_4SiC_4 grains was formed (Fig. 2f and Fig. 4d). However, the densification of these ceramic particles during the joining could not occur, due to a relatively low temperature, short time, and absence of external pressure (Fig. 2c). Therefore, the shear strength of the joint decreased to 38.3 ± 6.9 MPa, and failure occurred in the joining layer.

In conclusion, the successful joining of SiC ceramics was done using an ultra-fast Joule heating technique within a remarkably short timeframe of 23 s, achieved without the need for external pressure or pre-heating. The flash heating phenomenon was attributed to the rapid phase transformation generated via the interfacial reactions of the initial Al joining layer into high-resistance compounds, such as Al_4C_3, Al_4SiC_4, and Al_2OC. This localized heating mechanism, which inhibited the energy dissipation in heating the entire joint assembly, facilitated a sound SiC joints can be obtained within the remarkably short timeframe without external pressure and pre-heating, resulted in a maximum shear strength of 76 ± 12 MPa. The proposed approach, which utilizes the rapid increase in resistance associated with the phase transformation of the joining layer, presents significant potential for joining of wide range of ceramics, including carbides, oxides, nitrides, and/or ternary ceramics.

CRediT authorship contribution statement

Jie Xu: Writing – original draft, Visualization, Validation, Software, Methodology, Investigation, Formal analysis, Data curation. **Xiaobing Zhou:** Writing – review & editing, Writing – original draft, Supervision, Project administration, Methodology, Funding acquisition, Formal analysis, Conceptualization. **Qing Huang:** Writing – review & editing, Supervision, Conceptualization.

Declaration of competing interest

The authors declare that they have no known competing financial interests or personal relationships that could have appeared to influence the work reported in this paper.

Acknowledgements

This study was supported by the National Natural Science Foundation of China (Grant No U2330103, 11975296, and 12275337), Zhejiang Provincial Natural Science Foundation of China under Grant No LZ24A050004. We would like to recognize the support from the Ningbo Youth Science and Technology Innovation Leading Talent Project (2023QL043) and International Exchange Projects of the 9th Meeting of the China Slovakia Science and Technology Cooperation Committee (No. 9-6).

References

[1] Q. Liu, F. Ye, Y. Gao, S. Liu, H. Yang, Z. Zhou, Development of elongated 6H-SiC grains in reaction-bonded porous SiC ceramics, Scripta Mater 71 (2014) 13–16.
[2] R. He, N. Zhou, K. Zhang, X. Zhang, L. Zhang, W. Wang, D. Fang, Progress and challenges towards additive manufacturing of SiC ceramic, J. Adv. Ceram. 10 (2021) 637–674.
[3] P. Šajgalík, Z. Cheng, X. Han, C. Zhang, O. Hanzel, J. Sedláček, T. Orlova, M. Zhukovskyi, A.S. Mukasyan, Ultra-high creep resistant SiC ceramics prepared by rapid hot pressing, J. Eur. Ceram. Soc. 42 (2022) 820–829.
[4] T. Koyanagi, Y. Katoh, T. Nozawa, L.L. Snead, S. Kondo, C.H. Henager, M. Ferraris, T. Hinoki, Q. Huang, Recent progress in the development of SiC composites for nuclear fusion applications, J. Nucl. Mater. 511 (2018) 544–555.
[5] C. Song, F. Ye, L. Cheng, Y. Liu, Q. Zhang, Long-term ceramic matrix composite for aeroengine, J. Adv. Ceram. 11 (2022) 1343–1374.
[6] M. Liu, Q. Li, J. Hui, Y. Yan, R. Liu, B. Wang, Repelling effects of Mg on diffusion of He atoms towards surface in SiC: irradiation and annealing experiments combined with first-principles calculations, J. Adv. Ceram. 12 (2023) 2284–2299.

[7] T. Koyanagi, D.J. Sprouster, L.L. Snead, Y. Katoh, X-ray characterization of anisotropic defect formation in SiC under irradiation with applied stress, Scripta Mater 197 (2021) 113785.

[8] T. Koyanagi, Y. Katoh, T. Hinoki, C. Henager, M. Ferraris, S. Grasso, Progress in development of SiC-based joints resistant to neutron irradiation, J. Eur. Ceram. Soc. 40 (2020) 1023–1034.

[9] G. Liu, X. Zhang, J. Yang, G. Qiao, Recent advances in joining of SiC-based materials (monolithic SiC and SiC_f/SiC composites): joining processes, joint strength, and interfacial behavior, J. Adv. Ceram. 8 (2019) 19–38.

[10] J. Zhang, Y. Yan, P. Li, B. Wang, P. Wang, Z. Zhong, J. Lin, J. Cao, J. Qi, Unconventional joining techniques of ceramics by rapid heat sources: a review, J. Eur. Ceram. Soc. 43 (2023) 5748–5762.

[11] Y.H. Kim, Y.W. Kim, Direct bonding of silicon carbide ceramics sintered with yttria, J. Eur. Ceram. Soc. 39 (2019) 4487–4494.

[12] M. Li, X. Zhou, H. Yang, S. Du, Q. Huang, The critical issues of SiC materials for future nuclear systems, Scripta Mater 143 (2018) 149–153.

[13] S. Yang, X. Meng, B. Chen, Y. Ma, S. Kou, J. Deng, S. Fan, Encapsulation of SiC/SiC cladding tubes with excellent mechanical performance and air tightness using a CaO-modified Y_2O_3–Al_2O_3–SiO_2 glass, Ceram. Int. 50 (2024) 29850–29858.

[14] P. Li, Y. Yan, J. Lin, Y. Chen, P. Wang, Z. Wang, J. Tu, L. Qiao, Z. Zhong, J. Cao, J. Qi, Interfacial bonding mechanism and joint weakness area of brazed SiC and Nb with AuNi filler alloy: first-principles and experimental perspective, J. Am. Ceram. Soc. 106 (2023) 6255–6267.

[15] Y. Liu, Y. Zhu, Y. Yang, X. Liu, Z. Huang, Microstructure of reaction layer and its effect on the joining strength of SiC/SiC joints brazed using Ag-Cu-In-Ti alloy, J. Adv. Ceram. 3 (2014) 71–75.

[16] L. Zhou, C. Li, X. Si, C. Zhang, J. Qi, J. Cao, Flash brazing of SiC using Ag-Cu-Ti alloy at ultra-low temperature in air via electric field assistance, J. Eur. Ceram. Soc. 43 (2023) 7708–7713.

[17] P. Fitriani, B.-K. Min, D.-H. Yoon, Solid-state joining of SiC using a thin Ti_3AlC_2, TiC, or Ti filler, J. Eur. Ceram. Soc. 40 (2020) 2716–2720.

[18] S. He, L. Su, C. Zhan, X. Chen, W. Guo, S. Sun, L. Wu, J. Xue, H. Lin, Low-temperature joining of SiC ceramics by NITE phase using CaO-Al_2O_3-MgO-SiO_2 glass as an additive combined with surface oxidation, J. Eur. Ceram. Soc. 43 (2023) 5863–5870.

[19] C. Zhan, J. Wu, K. Huang, Y. Li, L. Wu, S. He, Y. Liu, Z. Zhang, W. Guo, J. Xue, H. Lin, Joining of textured PLS-SiC ceramic with CaO-Al_2O_3-MgO-TiO_2-SiO_2 glass filler, Ceram. Int. 50 (2024) 495–502.

[20] B. Tang, M. Wang, R. Liu, J. Liu, H. Du, A. Guo, A heat-resistant preceramic polymer with broad working temperature range for silicon carbide joining, J. Eur. Ceram. Soc. 38 (2018) 67–74.

[21] X. Zhou, Y. Han, X. Shen, S. Du, J. Lee, Q. Huang, Fast joining SiC ceramics with Ti_3SiC_2 tape film by electric field-assisted sintering technology, J. Nucl. Mater. 466 (2015) 322–327.

[22] X. Zhou, Z. Liu, Y. Li, Y. Li, P. Li, F. Huang, S. Ding, J. Lee, S. Du, Q. Huang, SiC ceramics joined with an in-situ reaction gradient layer of TiC/Ti_3SiC_2 and interface stress distribution simulations, Ceram. Int. 44 (2018) 15785–15794.

[23] X. Zhou, H. Yang, F. Chen, Y. Han, J. Lee, S. Du, Q. Huang, Joining of carbon fiber reinforced carbon composites with Ti_3SiC_2 tape film by Electric Field assisted sintering technique, Carbon N Y 102 (2016).

[24] P. Tatarko, Z. Chlup, A. Mahajan, V. Casalegno, T.G. Saunders, I. Dlouhý, M. J. Reece, High temperature properties of the monolithic CVD β-SiC materials joined with a pre-sintered MAX phase Ti_3SiC_2 interlayer via solid-state diffusion bonding, J. Eur. Ceram. Soc. 37 (2017) 1205–1216.

[25] L. Shi, X. Zhou, K. Xu, K. Chang, J. Dai, Z. Huang, Q. Huang, Low temperature seamless joining of SiC using a ytterbium film, J. Eur. Ceram. Soc. 41 (2021) 7507–7515.

[26] J. Xu, P. Tatarko, L. Chen, X. Shan, Q. Huang, X. Zhou, High-strength SiC joints fabricated at a low-temperature of 1400°C using a novel low activation filler of Praseodymium, J. Am. Ceram. Soc. 106 (2023) 5679–5688.

[27] X. Zhou, T. Yu, J. Xu, Y. Li, Z. Huang, Q. Huang, Ultrafast low-temperature near-seamless joining of C_f/SiC using a sacrificial $Pr3Si_2C_2$ filler via electric current field-assisted sintering technique, J. Eur. Ceram. Soc. 42 (2022) 6865–6875.

[28] X. Zhou, J. Liu, S. Zou, K. Xu, K. Chang, P. Li, F. Huang, Z. Huang, Q. Huang, Almost seamless joining of SiC using an in-situ reaction transition phase of $Y_3Si_2C_2$, J. Eur. Ceram. Soc. 40 (2020) 259–266.

[29] T. Yu, J. Xu, X. Zhou, P. Tatarko, Y. Li, Z. Huang, Q. Huang, Near-seamless joining of C_f/SiC composites using $Y_3Si_2C_2$via electric field-assisted sintering technique, J. Adv. Ceram. 11 (2022) 1196–1207.

[30] P. Tatarko, S. Grasso, T.G. Saunders, V. Casalegno, M. Ferraris, M.J. Reece, Flash joining of CVD-SiC coated C_f/SiC composites with a Ti interlayer, J. Eur. Ceram. Soc. 37 (2017) 3841–3848.

[31] M. Cologna, B. Rashkova, R. Raj, Flash sintering of Nanograin Zirconia in <5 s at 850°C, J. Am. Ceram. Soc. 93 (2010) 3556–3559.

[32] S. Sur, P.K. Tyagi, S.K. Jha, Flash sintering improves magnetic properties of spinel zinc ferrite, Scripta Mater 236 (2023) 115681.

[33] S. Molina-Molina, A. Perejón, L.A. Pérez-Maqueda, P.E. Sánchez-Jiménez, On the athermal origin of flash sintering: separating field-induced effects from joule heating using a current ramp approach, Scripta Mater 247 (2024) 116086.

[34] X. Su, W. Li, D. Chen, S. Zhang, C. Lou, Q. Tian, J. Zhao, P. Zhao, Rapid fabrication of oxygen-deficient zirconia by flash sintering treatment, J. Adv. Ceram. 13 (2024) 1881–1890.

[35] L. Lu, T. Liu, Z. Chen, F. Wang, M. Yang, Q. Wu, L. Yang, H. Li, Top priority current path between SiC particles during ultra-high temperature flash sintering: presence of PyC “bridges, J. Adv. Ceram. 13 (2024) 255–262.

[36] Y. Li, Q. Chi, Z. Yan, N. Yan, J. Liu, R. Huang, X. Wang, Flash sintering of high-purity alumina at room temperature, J. Adv. Ceram. 12 (2023) 2382–2388.

[37] L. Zhou, C. Li, X. Si, C. Zhang, B. Yang, J. Qi, J. Cao, Flash joining of SiC at ultra-low temperature, J. Eur. Ceram. Soc. 43 (2023) 2713–2717.

[38] M. Biesuz, V.M. Sglavo, Beyond flash sintering: how the flash event could change ceramics and glass processing, Scripta Mater 187 (2020) 49–56.

[39] Y.O Yoshitake, M. Kitayama, Joining of SiC ceramics by the flash-bonding technique, J. Mater. Sci. Chem. Eng. 8 (2020) 52–65.

[40] J.M. Lihrmann, J. Tirlocq, P. Descamps, F. Cambier, Thermodynamics of the Al–C–O system and properties of SiC–AlN–Al_2OC composites, J. Eur. Ceram. Soc. 19 (1999) 2781–2787.

[41] K. Liu, X. Huang, W. Yang, P. Wang, Study of the thermal stability of the Al_4SiC_4 phase via experiments and thermodynamic assessment, J. Alloys Compd. 976 (2024) 172967.

[42] D. Walter, I.W. Karyasa, Solid State reactions in the Al-Si-C system, J. Chin. Chem. Soc. 52 (2005) 873–876.

[43] J.C. Viala, P. Fortier, J. Bouix, Stable and metastable phase equilibria in the chemical interaction between aluminium and silicon carbide, J. Mater. Sci. 25 (1990) 1842–1850.

[44] X. Xing, B. Li, J. Chen, X. Hou, Formation mechanism of large size plate-like Al_4SiC_4 grains by a carbothermal reduction method, CrystEngComm 20 (2018) 1399–1404.

[45] J.M. Lihrmann, T. Zambetakis, M. Daire, High-temperature behavior of the aluminum oxycarbide Al_2OC in the system Al_2O_3–Al_4C_3 and with additions of aluminum nitride, J. Am. Ceram. Soc. 72 (1989) 1704–1709.

[46] W.R. King, R.C. Dorward, Electrical resistivity of aluminum carbide at 990–1240 K, J. Electrochem. Soc. 132 (1985) 388.

[47] K. Inoue, A. Yamaguchi, Temperature dependence of electrical resistivity of the Al_4SiC_4 sintered bodies prepared by pulse electronic current sintering, J. Ceram. Soc. Jpn. 111 (2003) 267–270.

[48] S. Grasso, T. Saunders, H. Porwal, B. Milsom, A. Tudball, M. Reece, Flash spark plasma sintering (FSPS) of α and β SiC, J. Am. Ceram. Soc. 99 (2016) 1534–1543.

[49] B. Guo, B. Chen, X. Zhang, X. Cen, X. Wang, M. Song, S. Ni, J. Yi, T. Shen, Y. Du, Exploring the size effects of Al_4C_3 on the mechanical properties and thermal behaviors of Al-based composites reinforced by SiC and carbon nanotubes, Carbon N Y 135 (2018) 224–235.

[50] G. Wen, X. Huang, Increased high temperature strength and oxidation resistance of Al_4SiC_4 ceramics, J. Eur. Cera. Soc. 26 (2006) 1281–1286.

[51] R. Arpón, J.M. Molina, R.A. Saravanan, C. García-Cordovilla, E. Louis, J. Narciso, Thermal expansion behaviour of aluminium/SiC composites with bimodal particle distributions, Acta Mater 51 (2003) 3145–3156.